Progress In Electromagnetics Research C, Vol. 128, 17–27, 2023

A Novel STAP Method with Enhanced Degrees of Freedom

Mingxin Liu[1, *], Wenying Feng[1], Jie Lin[2], Mengxu Fang[1], Wei Xu[1], and Xianding He[1]

Abstract—In this paper, a new space-time adaptive processing (STAP) method based on improved nested arrays and pulses configurations is proposed. Specifically, we first decompose the sensor array into two uniform linear arrays (ULAs) plus a separate sensor, similarly for pulse trains. Then, the original received signals from the physical array and pulse trains are introduced into the virtual domain, where the virtual clutter plus noise covariance matrix (CNCM) estimation is performed. Since the system has more virtual sensors and pulses from the perspective of virtual domain, the degrees of freedom (DOF) capability is effectively enhanced to improve the angle and Doppler resolution of radar. With the spatial-temporal smoothing technique, the STAP filter is designed by reconstructing the CNCM and virtual signal steering vector. Simulation results validate the effectiveness and superiority of the proposed algorithm.

1. INTRODUCTION

Space-time adaptive processing (STAP) is known to be a time-honored and valuable research topic, which has an excellent performance in clutter suppression and target detection [1–5]. As is known to all, the STAP performance is largely determined by the system degrees of freedom (DOF). Traditionally, researchers mainly focused on uniform linear arrays (ULAs), whose higher DOF usually requires more antenna sensors, leading to higher hardware cost and computational complexity [6–11]. To maximize the spatial resolution/DOF, the sparse arrays have attracted more attention than ULAs [12–15].

The research on sparse arrays and sparse pulse trains can be classified into two categories. The first category designs the system structure by considering an irregularly spaced array and interval pulse trains [12]. This type of method reduces the number of sensors and hardware resources at the expense of system performance. The second category can largely decrease the number of sensors and hardware complexity, increase the DOF, and improve system performance remarkably by using the fixed spaced array and fixed interval pulse, as well as the difference operator [13–15]. Sparse arrays such as (super) nested arrays [16–19], coprime arrays [14, 20–24], and minimum redundant arrays [25] can achieve greater DOF than the uniform linear array (ULA) in the same number of sensors. In other words, obtaining the same DOF, they need fewer sensors and hardware circuit.

In recent years, several STAP algorithms have been proposed by combining the difference operator, sparse arrays, and pulse trains [26–30]. The sparse STAP was proposed based on the concept of minimum redundancy structure to improve the performance of the system [26]. Because of the complexity of the minimum redundancy structure design, it is not practical for a large antenna array. To solve this problem, the coprime structure was applied to the STAP effectively in [27–29], which tries to improve the abilities of beamforming and target detection. It was later shown that through the use of (super) nest structures [16, 19, 30], one could also produce significant increase in DOF, and their uniform DOF is more than those of the coprime structure because coprime structure has holes in the virtual difference structure.

Received 18 September 2022, Accepted 27 October 2022, Scheduled 24 December 2022

* Corresponding author: Mingxin Liu (lmx0951@163.com).

[1] School of Unmanned Aerial Vehicles Industry, Chengdu Aeronautic Polytechnic, Chengdu 610100, China. [2] School of Aeronautics and Astronautics, Xihua University, Chengdu, Sichuan 610039, China.

In order to obtain more DOF, we present the optimal improved nested STAP (OIN-STAP) by using an improved nested structure [31] in the spatial and temporal domains. More concretely, the original space-time snapshots are obtained from the improved nested physical array and pulse trains structure. By using difference operator and spatial-temporal smoothing technology, the virtual space-time snapshots corresponding to the larger aperture ULA and the great many pulses with fixed pulse repetition interval (PRI) can be computed from the clutter plus noise covariance matrix (CNCM) obtained by the original received snapshots. Thus, a new virtual CNCM can be given for the STAP filter. Finally, the efficiencies of each strategies are analyzed, and the differences between them are compared, according to the simulation results obtained in the analog-digital computer system.

The rest of this paper is organized as follows. The concept of improved nested arrays and pulse trains is introduced in Section 2. In Section 3, we present the formulation of the OIN-STAP method. Simulation results are conducted in Section 4 to verify the superiority of the OIN-STAP. Finally, conclusions are presented in Section 5.

Notations: lowercase, bold lowercase, and bold capital letters represent scalars vectors and matrices, respectively. Transpose and complex conjugate transpose are denoted by $(\cdot)^T$ and $(\cdot)^H$, respectively. The symbols $\otimes$, $E(\cdot)$, and $|\cdot|$ stand for the Kronecker product, statistical expectation, and the absolute, respectively. $\mathbf{I}_M$ stands for the $M \times M$ identity matrix, and diag($\mathbf{a}$) represents a diagonal matrix whose diagonal elements are the column vector $\mathbf{a}$.

2. IMPROVED NESTED ARRAYS AND PRIS

In this section, we introduce the improved nested arrays and PRIs configuration.

2.1. Improved Nested Arrays

Improved nested arrays (INAs) consist of two ULAs and one single sensor, as shown in Fig. 1(a). In particular, one named inner ULA possesses N_1 sensors with spacing d and positions A_{in}. The other called outer ULA has N_2 sensors with spacing d_{out} and positions A_{out}, where $d_{out} = (N_1 + 2)d$. A single sensor is located in $(N_1 + 1)d$ position following the last sensor of outer ULA whose position set is represented by A_s. Thus, the sensor positions of INA can be expressed as

$$\mathrm{A} = \mathrm{A}_{in} \cup \mathrm{A}_{out} \cup \mathrm{A}_s \tag{1}$$

where

$$\mathrm{A}_{in} = \{n_{in}d,\ n_{in} = 0, 1, \ldots, N_1 - 1\} \tag{2}$$

$$\mathrm{A}_{out} = \{n_{out}(N_1 + 2)d + N_1 d,\ n_{out} = 0, \ldots, N_2 - 1\} \tag{3}$$

$$\mathrm{A}_s = \{(N_2 - 1)(N_1 + 2)d + N_1 d + (N_1 + 1)d\} \tag{4}$$

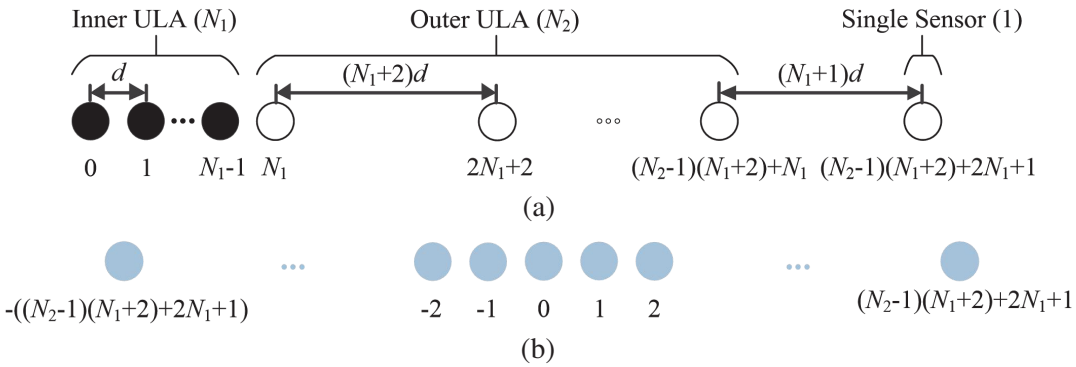

Figure 1. Improved nested arrays and the difference coarray. (a) Improved nested arrays. (b) The difference coarray.

It is obvious that the total number of sensors is $N = N_1 + N_2 + 1$. Here, the difference coarray D_A of an array A is defined as

$$\mathrm{D}_A = \{A_i - A_j | A_i, A_j \in \mathrm{A}\} \tag{5}$$

where A_i denotes the position of the ith sensor. Define set D_{AO} composed the different elements of D_A. Hence, the difference coarray D_{AO} of INA is a filled ULA with $\hat{N} = 2(N_2N_1 + 2N_2 + N_1) - 1$ in Fig. 1(b), and the virtual sensor positions for difference coarray are

$$\mathrm{D}_{AO} = \{nd \,|n = -N_c, \ldots, N_c,\ N_c = N_2N_1 + 2N_2 + N_1 - 1\} \tag{6}$$

In other words, we can obtain $2(N_2N_1+2N_2+N_1)-1$ DOF from only N_1+N_2+1 physical sensors by the difference operator.

Remarkably, the DOF of INA can be accurately calculated by the number of physical sensors. Therefore, we can gain the optimal values of N_1 and N_2 to maximize DOF under the given total number of sensors. At this time, the INA is described as optimal INA (OINA). In particular, when N is an even, and the maximum DOF of the difference coarray is $N^2/2 + 2N - 3$ in which $N_1 = N/2 - 1$ and $N_2 = N/2$. When N is odd, the optimal values of N_1 and N_2 are $(N-1)/2 - 1$ and $(N+1)/2$ respectively, and the corresponding maximum DOF is $N^2/2 + 2N - 7/2$.

2.2. Improved Nested PRIS

In order to further enhance DOF from the temporal dimension, PRIs can also adopt the improved nested structure. Improved nested PRI (IN-PRI) is composed of two uniform PRIs and one single pulse which is located in $(M_1 + 1)T_r$ position following the last pulse of outer PRI in a coherent processing interval (CPI) in Fig. 2(a), where two uniform PRIs can also be named as the inner PRI with M_1 and the outer PRI with M_2 whose minimal PRIs are T_r and $T_{out} = (M_1 + 2)T_r$, respectively. The total number of pulses is $M = M_1 + M_2 + 1$. Thus, the corresponding pulse positions are

$$\mathrm{P} = \mathrm{P}_{in} \cup \mathrm{P}_{out} \cup \mathrm{P}_s \tag{7}$$

where

$$\mathrm{P}_{in} = \{p_{in}T_r,\ p_{in} = 0, 1, \ldots, M_1 - 1\} \tag{8}$$

$$\mathrm{P}_{out} = \{p_{out}(M_1 + 2)T_r + M_1T_r,\ p_{out} = 0, \ldots, M_2 - 1\} \tag{9}$$

$$\mathrm{P}_s = \{(M_2 - 1)(M_1 + 2)T_r + M_1T_r + (M_1 + 1)T_r\} \tag{10}$$

are the pulse locations of the inner PRI, outer PRI, and one pulse, respectively. Similarly, the difference copulse D_P of the pulse trains P is

$$\mathrm{D}_{PO} = \{P_i - P_j \,|P_i, P_j \in \mathrm{P}\} \tag{11}$$

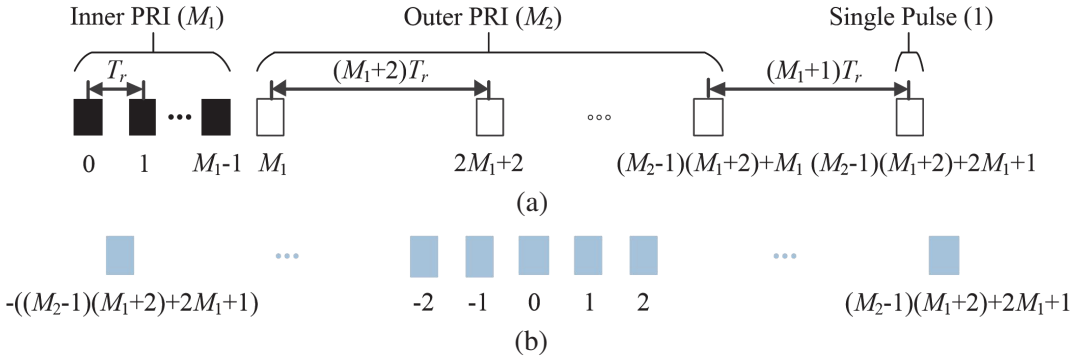

Figure 2. Improved nested PRIs and the difference copulse. (a) Improved nested PRIs. (b) The difference copulse.

where P_i means the location of the ith pulse. New set D_{PO} consists of different elements of D_P. Therefore, the difference copulse has $2(M_2M_1 + 2M_2 + M_1) - 1$ virtual pulses in Fig. 2(b) whose locations are given by

$$\mathrm{D}_{PO} = \{mT_r \,|m = -M_c, \ldots, M_c,\ M_c = M_2M_1 + 2M_2 + M_1 - 1\} \tag{12}$$

The above studies prove that IN-PRI can also achieve $2(M_2M_1+2M_2+M_1)-1$ DOF with M_1+M_2+1 physical pulses in the temporal dimension.

From the analysis for the INA here we see that optimal IN-PRI (OIN-PRI) has $M^2/2 + 2M - 3$ DOF if the total number of pulses $M = M_1 + M_2 + 1$ is even in which $M_1 = M/2 - 1$ and $M_2 = M/2$. When M is odd, the DOF is $M^2/2 + 2M - 7/2$ with $M_1 = (M-1)/2 - 1$ and $M_2 = (M+1)/2$.

3. THE PROPOSED METHOD

In this section, we firstly develop a new STAP with the improved nested structure, then use the virtual sensors and pulse trains to construct the virtual space-time snapshot, and finally design the STAP filter.

3.1. Signal Model

Assume that a side-looking airborne phased array radar has N receiving elements and M transmitting pulses in a CPI, where the receiving array and transmitting pulse for radar are configured as improved nested structure. $d = \lambda/2$ is the minimum inter-element spacing, T_r the minimal PRI, and λ the radar wavelength [1]. The received space-time snapshots from a range bin without the ranger ambiguity can be given by

$$\mathbf{x} = a_t\mathbf{v}(\phi_t, f_t) + \mathbf{x}_u \tag{13}$$

where a_t denotes the target complex gain. The target space-time steering vector is $\mathbf{v}(f_t, \phi_t) = \mathbf{v}(f_t) \otimes \mathbf{v}(\phi_t)$, and $\mathbf{v}(\phi_t)$ and $\mathbf{v}(f_t)$ denote the target spatial and temporal steering vectors, respectively, defined as

$$\mathbf{v}(\phi_t) = \left[1, e^{2\pi j n_1\phi_t}, \ldots, e^{2\pi j n_{N-1}\phi_t}\right]^T \tag{14}$$

$$\mathbf{v}(f_t) = \left[1, e^{2\pi j m_1 f_t}, \ldots, e^{2\pi j m_{M-1} f_t}\right]^T \tag{15}$$

where $f_t = 2v_rT_r\cos(\theta)/\lambda$ and $\phi_t = d\cos(\theta)/\lambda$, v_r is the velocity of the radar, and θ is the target directions. $\mathbf{x}_u$ is the clutter plus noise data, expressed by

$$\mathbf{x}_u = \sum_{i=1}^{N_c} a_{c,i}\mathbf{v}(\phi_{c,i}, f_{c,i}) + \mathbf{n} = \sum_{i=1}^{N_c} a_{c,i}\mathbf{v}(\phi_{c,i}) \otimes \mathbf{v}(f_{c,i}) + \mathbf{n} \tag{16}$$

where $\mathbf{n}$ is the Gaussian white noise vector whose power is σ_n^2; N_c is the number of independent clutter patches in azimuth domain; $f_{c,i}$ and $\phi_{c,i}$ are the normalized Doppler and spatial frequency of the ith clutter patch, respectively; $a_{c,i}$ is the ith clutter patch complex gain. The ith clutter patch corresponding spatial and temporal steering vectors are defined by respectively

$$\mathbf{v}(\phi_{c,i}) = \left[1, e^{2\pi j n_1\phi_{c,i}}, \ldots, e^{2\pi j n_{N-1}\phi_{c,i}}\right]^T \tag{17}$$

$$\mathbf{v}(f_{c,i}) = \left[1, e^{2\pi j m_1 f_{c,i}}, \ldots, e^{2\pi j m_{M-1} f_{c,i}}\right]^T \tag{18}$$

c, i is the corresponding space-time steering vector and can be computed as

$$\mathbf{v}(\varphi_{c,i}, f_{c,i}) = \begin{bmatrix} 1 \\ e^{2\pi j n_1\varphi_{c,i}} \\ \vdots \\ e^{2\pi j n_{N-1}\varphi_{c,i}} \end{bmatrix} \otimes \begin{bmatrix} 1 \\ e^{2\pi j m_1 f_{c,i}} \\ \vdots \\ e^{2\pi j m_{M-1} f_{c,i}} \end{bmatrix} = \begin{bmatrix} v_{0,i} \\ v_{1,i} \\ \vdots \\ v_{NM-1,i} \end{bmatrix} \tag{19}$$

where $v_{lM+r-1,i} = e^{2\pi j(n_l\phi_{c,i}+m_{r-1}f_{c,i})}$, $l = 0,\ldots,N-1$, $r = 1,\ldots,M$, $i = 1,\ldots,N_c$. Assuming that different clutter patches are independent, the CNCM based on (16) can be modelled as follows:

$$\begin{aligned}\mathbf{R}_u &= E\left[\mathbf{x}_u\mathbf{x}_u^H\right] \\ &= \sum_{i=1}^{N_c} E\left(|a_{c,i}|^2\right)\mathbf{v}\left(\phi_{c,i},f_{c,i}\right)\mathbf{v}^H\left(\phi_{c,i},f_{c,i}\right)+\sigma_n^2\mathbf{I}_{NM} \\ &= \mathbf{V}\mathbf{P}\mathbf{V}^H+\sigma_n^2\mathbf{I}_{NM}\end{aligned} \tag{20}$$

where $\mathbf{V} = [\mathbf{v}(\phi_{c,1},f_{c,1}),\mathbf{v}(\phi_{c,2},f_{c,2}),\ldots,\mathbf{v}(\phi_{c,N_c},f_{c,N_c})]$ is the clutter space-time steering matrix, and the clutter power matrix is $\mathbf{P} = \mathrm{diag}([p_1,p_2,\ldots,p_{N_c}]^T)$, $p_k = E(|a_{c,k}|^2)$. Combining (19) with (20), the clutter covariance matrix (CCM) can be calculated by

$$\mathbf{R}_c = \mathbf{V}\mathbf{P}\mathbf{V}^H = \begin{bmatrix} R_{0,0} & R_{0,1} & \cdots & R_{0,NM-1} \\ R_{1,0} & R_{1,1} & \cdots & R_{1,NM-1} \\ \vdots & \vdots & \ddots & \vdots \\ R_{NM-1,0} & R_{NM-1,1} & \cdots & R_{NM-1,NM-1} \end{bmatrix} \tag{21}$$

where $R_{(l_1M+r_1-1),(l_2M+r_2-1)} = \sum\limits_{k=1}^{N_c} p_k e^{2\pi j[(n_{l_1}-n_{l_2})\phi_{c,k}+(m_{r_1-1}-m_{r_2-1})f_{c,k}]}$, $l_1,l_2 = 0,\ldots,N-1$, $r_1,r_2 = 1,\ldots,M$.

3.2. Virtual Space-Time Snapshot Construction

In order to obtain the optimal weight vector, the term $R_{(l_1M+r_1-1),(l_2M+r_2-1)}$ on (21) can be rewritten as

$$R_{(l_1M+r_1-1),(l_2M+r_2-1)} = \sum_{k=1}^{N_c} p_k e^{2\pi j\left[\left(n_{l_1}-n_{l_2}\right)\phi_{c,k}\right]} e^{2\pi j\left[\left(m_{r_1-1}-m_{r_2-1}\right)f_{c,k}\right]} \tag{22}$$

where $\hat{n}_{kl}$=$n_{l_1}-n_{l_2}$ can be regarded as the array positions of the difference coarray from (5). The set $\{\hat{n}\}$ consists of unique continuous integers of the set $\{\hat{n}_{kl}\}$. Predictably, the continuous difference coarray can be equivalent to a virtual ULA composed of $\hat{N} = 2\bar{N}+1$ sensors with $\hat{n}d$ spacing. The set $\hat{n}$ is

$$\hat{n} = \left\{-\bar{N},-\bar{N}+1,\ldots,\bar{N}-1,\bar{N}\right\}\left(\bar{N} = N_2N_1+2N_2+N_1-1\right) \tag{23}$$

where $\hat{p}_{kl} = p_k - p_l$ can be regarded as the pulse positions of the difference copulse. The set $\{\hat{p}\}$ is made up of unique continuous integers of the set $\{\hat{p}_{kl}\}$. The difference copulse resembles a virtual CPI composed of $\hat{P} = 2\bar{M}+1$ pulses with $\hat{p}T_r$ spacing. The set $\hat{p}$ is

$$\hat{p} = \left\{-\bar{M},-\bar{M}+1,\ldots,\bar{M}-1,\bar{M}\right\}\left(\bar{M} = M_2M_1+2M_2+M_1-1\right) \tag{24}$$

$\widehat{\mathbf{v}}(\phi_{c,i})$ and $\widehat{\mathbf{v}}(f_{c,i})$ are the corresponding virtual spatial and Doppler steering vectors and can be defined respectively by

$$\widehat{\mathbf{v}}(\phi_{c,i}) = \left[e^{-j2\pi\phi_{c,i}\bar{N}},\ldots 1,\ldots,e^{j2\pi\phi_{c,i}\bar{N}}\right]^T \tag{25}$$

$$\widehat{\mathbf{v}}(f_{c,i}) = \left[e^{-j2\pi f_{c,i}\bar{M}},\ldots 1,\ldots,e^{j2\pi f_{c,i}\bar{M}}\right]^T \tag{26}$$

Consequently, the virtual space-time snapshot $\mathbf{Y}$ form $\mathbf{R}_u$ can be given by

$$\mathbf{Y} = \sum_{i=1}^{N_c} E\left(|a_{c,i}|^2\right)\widehat{\mathbf{v}}\left(\phi_{c,i}\right)\widehat{\mathbf{v}}^T\left(f_{c,i}\right)+\sigma_n^2\mathbf{e}_1\mathbf{e}_2^T \tag{27}$$

where the elements of $\mathbf{e}_1 \in C_{\hat{N}\times 1}$ and $\mathbf{e}_2 \in C_{\hat{P}\times 1}$ are all zeros except the one in the center position. Vectoring (27), we can get a virtual space-time snapshot which can be written as

$$\begin{aligned}\mathbf{y} &= \sum_{i=1}^{N_c} E\left(|a_{c,i}|^2\right)\widehat{\mathbf{v}}\left(f_{c,i}\right)\otimes\widehat{\mathbf{v}}\left(\phi_{c,i}\right)+\sigma_n^2\mathbf{e}_2\otimes\mathbf{e}_1 \\ &= \sum_{i=1}^{N_c} E\left(|a_{c,i}|^2\right)\widehat{\mathbf{v}}_{ci}+\sigma_n^2\widehat{\mathbf{e}} = \widehat{\mathbf{c}}+\widehat{\mathbf{n}}\end{aligned} \tag{28}$$

where $\widehat{\mathbf{e}} = \mathbf{e}_2\otimes\mathbf{e}_1$. $\widehat{\mathbf{v}}_{ci} = \widehat{\mathbf{v}}(f_{c,i})\otimes\widehat{\mathbf{v}}(\phi_{c,i})$, $\widehat{\mathbf{c}}$, and $\widehat{\mathbf{n}}$ denote the virtual space-time steering vector, clutter vector, and noise vector, respectively.

3.3. Virtual Clutter Plus Noise Covariance Matrix Estimation

To estimate the filter weight, we can get a virtual CNCM estimation by spatial-temporal smoothing technology. The submatrices $\mathbf{Y}_{\rho,\gamma}$ from $\mathbf{Y}$ can be defined as

$$\mathbf{Y}_{\rho,\gamma} = \sum_{i=1}^{N_c} e^{-j(\rho\phi_{c,i}+\gamma f_{c,i})}E\left(|a_{c,i}|^2\right)\bar{\mathbf{v}}\left(\phi_{c,i}\right)\bar{\mathbf{v}}\left(f_{c,i}\right)^T+\sigma_n^2\mathbf{e}_{1,\rho}\mathbf{e}_{2,\gamma}^T \tag{29}$$

where $\mathbf{e}_{1,\rho}$ is a subvector formed from the $(\bar{N}+1-\rho)$th to $(2\bar{N}+1-\rho)$th entries of $\mathbf{e}_1$, and $\mathbf{e}_{2,\gamma}$ is a subvector formed from $(\bar{M}+1-\gamma)$ to $(2\bar{M}+1-\gamma)$ entry of $\mathbf{e}_2$, $\rho = 0,1,\ldots,\bar{N}$ and $\gamma = 0,1,\ldots,\bar{M}$. $\bar{\mathbf{v}}(\phi_{c,i})$ and $\bar{\mathbf{v}}(f_{c,i})$ can be seen as the spatial and Doppler steering vectors corresponding to a virtual sub-ULA and sub-CPI.

Then, we can obtain a new covariance matrix by vectoring $\mathbf{Y}_{\rho,\gamma}$, which is formulated as

$$\mathbf{R}_{vs} = \frac{1}{\left(\bar{N}+1\right)\left(\bar{M}+1\right)}\sum_{\rho=0}^{\bar{N}}\sum_{\gamma=0}^{\bar{M}}\mathbf{y}_{\rho,\gamma}\mathbf{y}_{\rho,\gamma}^H \tag{30}$$

According to [17], (30) can be rewritten as

$$\mathbf{R}_{vs} = \frac{1}{\left(\bar{N}+1\right)\left(\bar{M}+1\right)}\left(\bar{\mathbf{V}}_c\mathbf{P}\bar{\mathbf{V}}_c^H+\sigma_n^2\mathbf{I}_{(\bar{N}+1)(\bar{M}+1)}\right)^2 \tag{31}$$

where $\bar{\mathbf{V}}_c = [\bar{\mathbf{v}}(\phi_{c,1},f_{c,1}),\bar{\mathbf{v}}(\phi_{c,2},f_{c,2}),\ldots,\bar{\mathbf{v}}(\phi_{c,N_c},f_{c,N_c})]$. From (27), we have

$$\mathbf{R}_{vr} = \left(\bar{\mathbf{V}}_c\mathbf{P}\bar{\mathbf{V}}_c^H+\sigma_n^2\mathbf{I}_{(\bar{N}+1)(\bar{M}+1)}\right) = \left(\left(\bar{N}+1\right)\left(\bar{M}+1\right)\mathbf{R}_{vs}\right)^{1/2} \tag{32}$$

Thus, the optimum filter weight corresponding to (32) can be expressed as follows:

$$\bar{\mathbf{w}} = \frac{\mathbf{R}_{vr}^{-1}\bar{\mathbf{v}}_t}{\bar{\mathbf{v}}_t^H\mathbf{R}_{vr}^{-1}\bar{\mathbf{v}}_t} \tag{33}$$

where $\bar{\mathbf{v}}_t$ is the target virtual space-time steering vector.

3.4. DOF

Obtained by the above derivation, improved nested arrays and PRIs structure can be transformed into a virtual uniform ULA and PRI model, and its DOF has the form as follows:

$$\hat{D} = \hat{N}\hat{P} = \left(2\bar{N}+1\right)\times\left(2\bar{M}+1\right) \tag{34}$$

Due to the space-time smoothing technology, however, the final DOF of the filter is reduced to

$$D = \left(\bar{N}+1\right)\left(\bar{P}+1\right) = \left(N_2N_1+2N_2+N_1\right)\times\left(M_2M_1+2M_2+M_1\right) \tag{35}$$

which is less than $\hat{D}$, but larger than NP. The system possesses the maximum DOF when it runs with the OINA and OIN-PRI strategy at the same time, which is called OIN-STAP. Then, the DOF of filter can be computed by

$$D_{opt} = \begin{cases} \left(\frac{N}{4}^2 + N - \frac{5}{4}\right) \times \left(\frac{M}{4}^2 + M - \frac{5}{4}\right) & if \quad N \text{ is odd, } M \text{ is odd} \\ \left(\frac{N}{4}^2 + N - 1\right) \times \left(\frac{M}{4}^2 + M - 1\right) & if \quad N \text{ is even, } M \text{ is even} \\ \left(\frac{N}{4}^2 + N - \frac{5}{4}\right) \times \left(\frac{M}{4}^2 + M - 1\right) & if \quad N \text{ is odd, } M \text{ is even} \\ \left(\frac{N}{4}^2 + N - 1\right) \times \left(\frac{M}{4}^2 + M - \frac{5}{4}\right) & if \quad N \text{ is even, } M \text{ is odd} \end{cases} \tag{36}$$

From this point of view, the OIN-STAP filter can obtain the $O(N^2M^2)$ DOF from $O(NM)$ physical sensors and pulses.

4. SIMULATION RESULTS

In this section, we perform comprehensive comparisons between the existing methods including the traditional STAP (T-STAP) [1], coprime STAP (C-STAP) [29], second-order (super) nested STAP (N-STAP) [16, 19], and OIN-STAP by numerical experiments. Consider that a side-looking airborne radar is configured with $N = 10$, $M = 10$, $\lambda = 0.05\,\text{m}$, $T_r = 0.25\,\text{ms}$, $N_c = 361$, $v = 50\,\text{m/s}$, and $\sigma_n^2 = 1$. The number of samples is $L = 200$. For the coprime STAP, we set $N_1 = M_1 = 3$ and $N_2 = M_2 = 5$. The specific parameters for the second-order nested STAP are $N_1 = M_1 = 5$ and $N_2 = M_2 = 5$. To maximize DOF, the proposed method has $N_1 = M_1 = 4$ and $N_2 = M_2 = 5$. Assume that the normalized angle and Doppler frequency of target are 0.1 and -0.2, respectively. The clutter to noise ratio in the simulation is set to 30 dB, and the signal to noise ratio is 0 dB. All simulation results are averages over 100 Monte Carlo experiments.

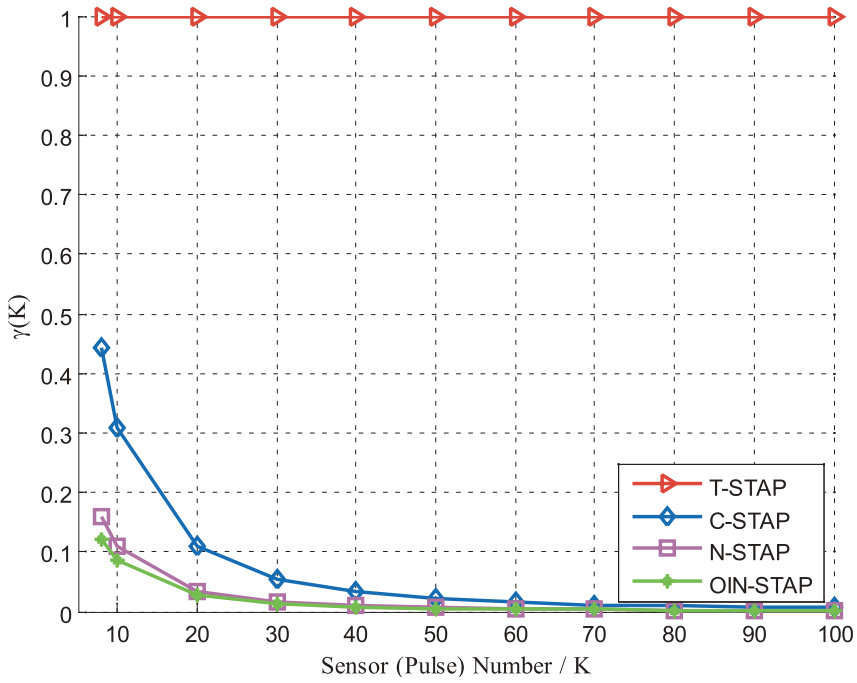

Figure 3. The DOF ratiao with the sensor/pulse number K varying from 8 to 100.

4.1. DOF

First, we prove the ability of the various STAP methods to improve DOF with the given numbers of sensors and pulses. For the purpose of generalizing this discussion, we assume that the total numbers of sensors and pulses are both K, i.e., $M = N = K$. Here we define the DOF ratio as [27]

$$\gamma(K) = K^2/L(K) \tag{37}$$

where $L(K)$ represents the maximum DOF of STAP filter. The smaller the $\gamma(K)$ is, the higher the DOF is. Fig. 3 reveals the $\gamma(K)$ of four methods by varying K from 8 to 100. The C-STAP, N-STAP, and OIN-STAP have higher DOF than T-STAP. In particular, the OIN-STAP has the higher DOF than the other three methods in fixed K. Furthermore, $\gamma(K)$ of OIN-STAP are close to 0 in small K which means that the OIN-STAP can provide greater DOF by a few sensors and pulses.

4.2. Beampatterns in Spatial and Temporal Domain

Next, we demonstrate the capability to form beams in the separated spatial or temporal domain. Fig. 4(a) gives the beampattern in the spatial domain at the target normalized Doppler frequency while

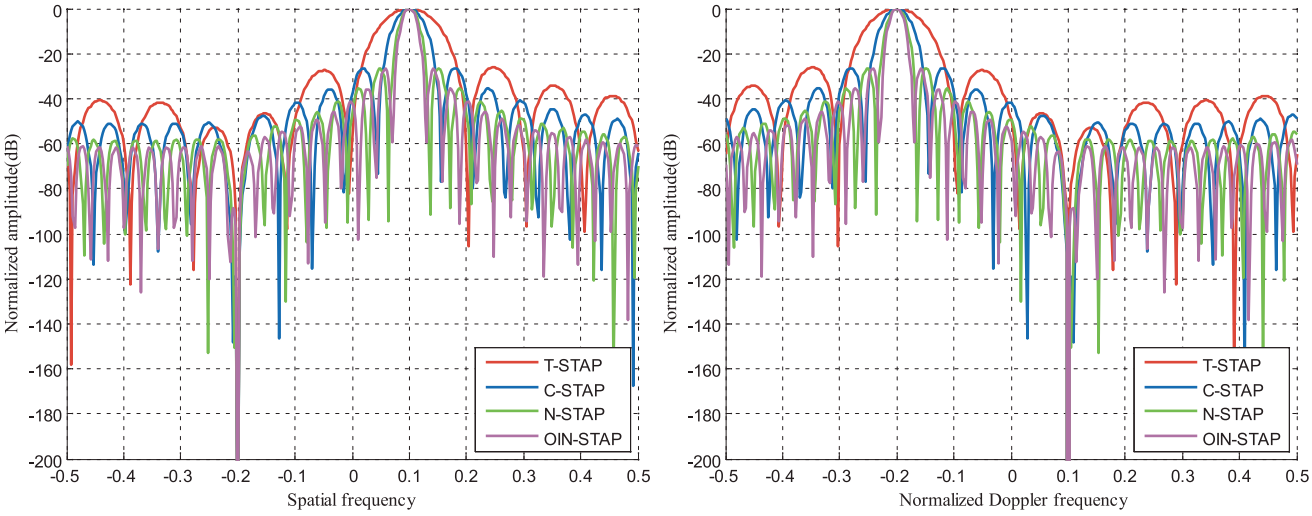

Figure 4. Beampatterns. (a) Spatial domain. (b) Doppler domain.

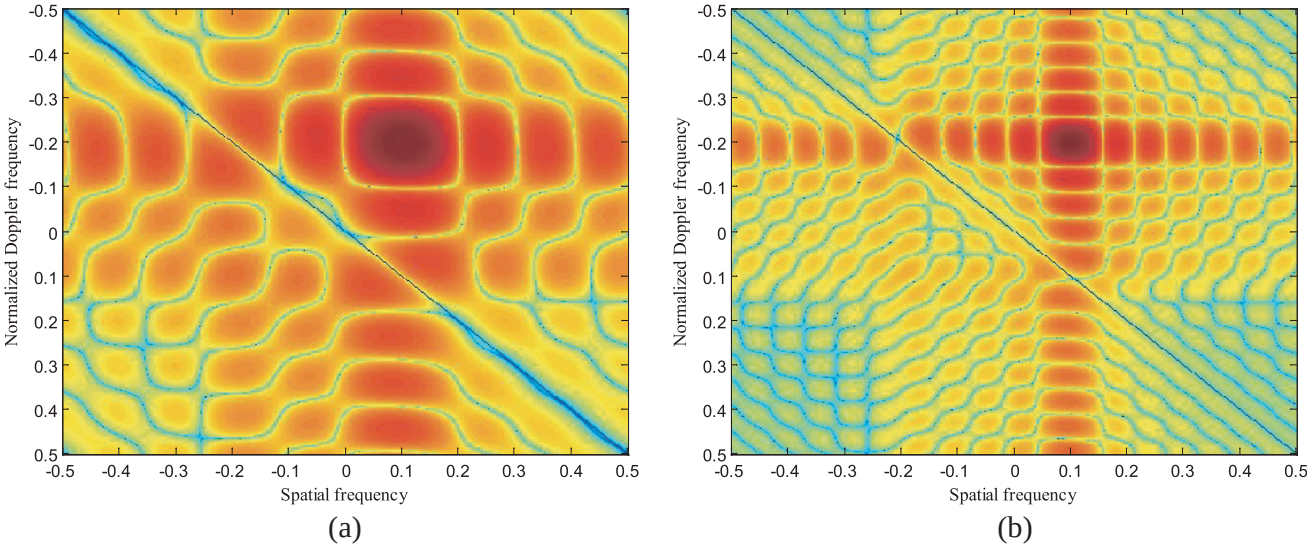

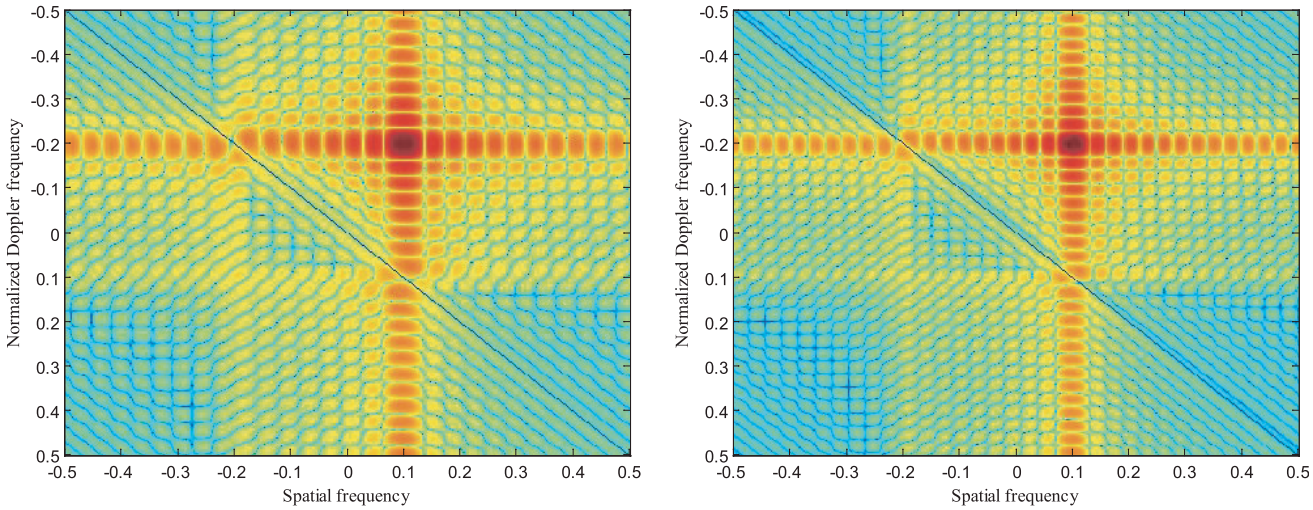

Figure 5. Space time Beampatterns. (a) T-STAP. (b) C-STAP. (c) N-STAP. (d) OIN-STAP.

Fig. 4(b) shows the beampattern in Doppler domain at the target normalized spatial frequency. It can be observed from Fig. 4 that the OIN-STAP provides high-quality beampatterns in the separated spatial and temporal domains. In particular, it has the narrowest main lobe among all these STAP methods. This is because the virtual DOF of the OIN-STAP is larger than those of any other array and pulse geometries.

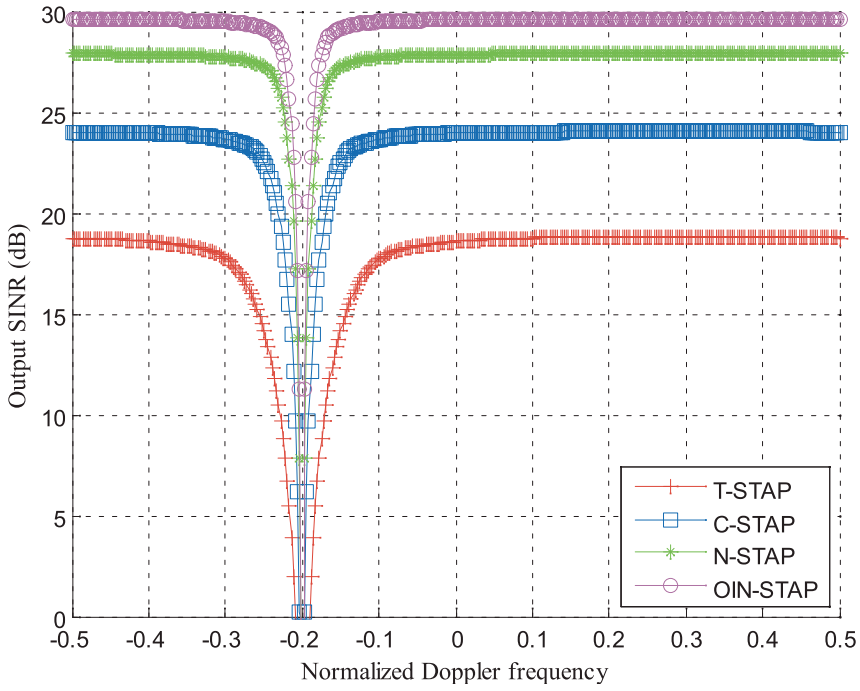

Figure 6. Output SINR.

4.3. Space-Time Beampatterns

Third, Fig. 5 shows the space time beampatterns. It is deduced from Fig. 5 that the functions of four ways are basically the same. They form a deep notch on the clutter ridge and detect the precise location of the target. There are obvious wide main lobe and high side lobe level in the estimated result by using the T-STAP due to its limited DOF capacity. The C-STAP possesses higher DOFs; therefore, their performances are moderately improved. Its detection performance is still lower than N-STAP. The OIN-STAP gains greater DOF than the other three methods, and as a result, its side-lobe level and angle-Doppler resolution are optimal.

4.4. SINR

Finally, we assess the output SINR performance against the normalized Doppler frequency. As depicted in Fig. 6, the compared output SINR chart is shown for the SINR performance of four different models, including the T-STAP, C-STAP, N-STAP, and OIN-STAP. The theoretical upper bound of output SINR for the T-STAP is at the lowest level due to its limited DOF capacity. The C-STAP and N-STAP possess higher DOF; therefore, their output SINR performances are moderately improved. The OIN-STAP has the maximum DOF compared with the other three algorithms, and as a result, it achieves the best SINR performance.

5. CONCLUSIONS

We propose a novel STAP method in this paper by extending the concept of second-order nested STAP. The proposed STAP method is able to achieve more DOF than those of the existing STAP, which is more effective than traditional techniques on contributions to raising the capability of parameters estimation, especially to raising the precision of signal detection in space dimension and time dimension at the same time. Simulation results indicate the effectiveness and good performance of our proposed STAP.

REFERENCES

1. Li, J. and P. Stoica, *MIMO Radar Signal Processing*, Wiley, Hoboken, NJ, USA, 2009.
2. Liu, M., X. Wang, and L. Zou, "Robust STAP with reduced mutual coupling and enhanced DOF based on super nested sampling structure," *IEEE Access*, Vol. 7, 175420–175428, 2019.
3. Wei, W., L. Zou, and X. Wang, "Research on space-time adaptive processing with respect to the signal powers," *Progress In Electromagnetics Research C*, Vol. 82, 99–107, 2018.
4. Wei, W., L. Zou, and X. Wang, "An array partitioning scheme of airborne phased-MIMO radar based on STAP SINR," *Progress In Electromagnetics Research Letters*, Vol. 79, 95–101, 2018.
5. Liu, M., L. Zou, X. Yu, Y. Zhou, X. Wang, and B. Tang, "Knowledge aided covariance matrix estimation via Gaussian kernel function for airborne SR-STAP," *IEEE Access*, Vol. 8, 5970–5978, Jan. 2020.
6. Cai, W., H. Yan, J. Peng, J. Wu, et al., "Slow-time FDA-MIMO technique with application to STAP radar," *IEEE Trans. Aerosp. Electron. Syst.*, Vol. 58, No. 1, 74–95, 2022.
7. Jiang, Z., Y. He, G. Li, and X. Zhang, "Robust STAP detection based on volume cross-correlation function in heterogeneous environments," *IEEE Geosci. Remote Sens. Lett.*, Vol. 19, 2022.
8. Ma, H., H. Tao, J. Su, and B. Liao, "DOD/DOA and polarization estimation in MIMO systems with spatially spread dipole quints," *IEEE Commun. Lett.*, Vol. 24, 99–102, Jan. 2020.
9. Fishler, E., A. Haimovich, R. S. Blum, L. J. Cimini, D. Chizhik, and R. A. Valenzuela, "Spatial diversity in radars — Models and detection performance," *IEEE Trans. Signal Process.*, Vol. 54, No. 3, 823–838, Mar. 2006.
10. Li, J. and P. Stoica, "MIMO radar with colocated antennas," *IEEE Signal Process. Mag.*, Vol. 24, No. 5, 106–114, Sep. 2007.

11. Bekkerman, I. and J. Tabrikian, "Target detect-ion and localization using MIMO radars and sensors," *IEEE Trans. Signal Process.*, Vol. 54, No. 10, 3873–3883, Oct. 2006.
12. Liu, Z., X. Wei, and X. Li, "Aliasing-free moving target detection in random pulse repetition interval radar based on compressed sensing," *IEEE Sensors J.*, Vol. 13, No. 7, 2523–2534, Jul. 2013.
13. Pal, P. and P. Vaidyanathan, "Nested arrays: A novel approach to array processing with enhanced degrees of freedom," *IEEE Trans. Signal Process.*, Vol. 58, No. 8, 4167–4181, Aug. 2010.
14. Vaidyanathan, P. and P. Pal, "Sparse sensing with coprime samplers and arrays," *IEEE Trans. Signal Process.*, Vol. 59, No. 2, 573–586, Feb. 2011.
15. Liu, C.-L. and P. Vaidyanathan, "Remarks on the spatial smoothing step in coarray MUSIC," *IEEE Signal Process. Lett.*, Vol. 22, No. 9, 1438–1442, Sep. 2015.
16. Liu, M., X. Wang, and L. Zou, "Robust STAP with reduced mutual coupling and enhanced DOF based on super nested sampling structure," *IEEE Access*, Vol. 7, 175420–175428, 2019.
17. Pal, P. and P. P. Vaidyanathan, "Nested arrays in two dimensions, Part II: Application in two dimensional array processing," *IEEE Trans. Signal Process.*, Vol. 60, No. 9, 4706–4718, Sept. 2012.
18. Liu, C.-L. and P. P. Vaidyanathan, "Super nested arrays: Linear sparse arrays with reduced mutual coupling — Part I: Fundamentals," *IEEE Trans. Signal Process.*, Vol. 64, No. 15, 3997–4012, Aug. 2016.
19. Wang, W., L. Zou, and X. Wang, "A novel two-level nested STAP strategy for clutter suppression in airborne radar," *Math. Problems Eng.*, Vol. 2019, Art. No. 2540858, Jun. 2019.
20. Liu, C.-L. and P. P. Vaidyanathan, "Cramér-Rao bounds for coprime and other sparse arrays, which find more sources than sensors," *Digital Signal Process.*, Vol. 61, 43–61, 2016.
21. Zheng, G. and J. Tang, "DOD and DOA estimation in bistatic MIMO radar for nested and coprime array with closed-form DOF," *Int. J. Electron.*, Vol. 104, No. 5, 885–897, Nov. 2016.
22. Qin, S., Y. Zhang, and M. Amin, "Generalized coprime array configurations for direction-of-arrival estimation," *IEEE Trans. Signal Process.*, Vol. 63, No. 6, 1377–1390, Mar. 2015.
23. Tan, Z., Y. Eldar, and A. Nehorai, "Direction of arrival estimation using co-prime arrays: A super resolution viewpoint," *IEEE Trans. Signal Process.*, Vol. 62, No. 21, 5565–5576, Nov. 2014.
24. Adhikari, K., J. R. Buck, and K. E. Wage, "Extending coprime sensor arrays to achieve the peak side lobe height of a full uniform linear array," *EURASIP J. Adv. Signal Process.*, Vol. 2014, No. 1, 2014.
25. Moffet, A. T., "Minimum-redundancy linear arrays," *IEEE Trans. Antennas Propag.*, Vol. 16, No. 2, 172–175, 1968.
26. Li, R., Y. Wang, Z. He, J. Li, and G. Sun, "Minimum redundancy space-time adaptive processing utilizing reconstructed covariance matrix," *Proc. IEEE Radar Conf. (RadarConf)*, 0722–0726, Seattle, WA, USA, 2017.
27. Liu, C.-L. and P. P. Vaidyanathan, "Coprime arrays and samplers for space-time adaptive processing," *Proc. IEEE Int. Conf. Acoust. Speech, Signal Procces. (ICASSP)*, 2364–2368, Queensland, Australia, 2015.
28. Liu, S., Y. Ma, and T. Shan, "Segmented discrete polynomial-phase transform with coprime sampling," *Proc. IET Int. Radar Conf. (IRC)*, 5619–5621, Nanjing, Jiangsu, China, 2018.
29. Wang, X., Z. Yang, H. Huang, J. Huang, and M. Jiang, "Space-time adaptive processing for airborne radars with space-time coprime sampling structure," *IEEE Access*, Vol. 6, 20031–20046, Apr. 2018.
30. Vouras, P., "Fully adaptive space-time processing on nested arrays," *Proc. IEEE Radar Con. (RadarCon)*, 0858–0863, Arlington, VA, USA, 2015.
31. Yang, M., L. Sun, X. Yuan, and B. Chen, "Improved nested array with hole-free DCA and more degrees of freedom," *IEEE Trans. Signal Process.*, Vol. 52, No. 25, 2068–2070, Dec. 2016.